Geomechanics and Engineering, *Vol. 16, No. 3 (2018) 273-284*
DOI: https://doi.org/10.12989/gae.2018.16.3.273

Experimental investigation of the mechanical behaviors of grouted crushed coal rocks under uniaxial compression

Yuhao Jin[1,2,4], Lijun Han[*1,2], Qingbin Meng[2], Dan Ma[3], Shengyong Wen[1] and Shuai Wang[2]

[1]*School of Mechanics and Civil Engineering, China University of Mining and Technology, Xuzhou, Jiangsu 221116, China*
[2]*State Key Laboratory for Geomechanics and Deep Underground Engineering, China University of Mining and Technology, Xuzhou, Jiangsu 221116, China*
[3]*School of Resources & Safety Engineering, Central South University, Changsha, Hunan 410083, China*
[4]*GeoEnergy Research Centre (GERC), University of Nottingham, Nottingham, NG7 2RD, U.K.*

(Received March 23, 2017, Revised February 28, 2018, Accepted June 15, 2018)

Abstract. A detailed understanding of the mechanical behaviors for crushed coal rocks after grouting is a key for construction in the broken zones of mining engineering. In this research, experiments of grouting into the crushed coal rock using independently developed test equipment for solving the problem of sampling of crushed coal rocks have been carried out. The application of uniaxial compression was used to approximately simulate the ground stress in real engineering. In combination with the analysis of crack evolution and failure modes for the grouted specimens, the influences of different crushed degrees of coal rock (CDCR) and solidified grout strength (SGS) on the mechanical behavior of grouted specimens under uniaxial compression were investigated. The research demonstrated that first, the UCS of grouted specimens decreased with the decrease in the CDCR at constant SGS (except for the SGS of 12.3 MPa). However, the UCS of grouted specimens for constant CDCR increased when the SGS increased; optimum solidification strengths for grouts between 19.3 and 23.0 MPa were obtained. The elastic moduli of the grouted specimens with different CDCR generally increased with increasing SGS, and the peak axial strain showed a slightly nonlinear decrease with increasing SGS. The supporting effect of the skeleton structure produced by the solidified grouts was increasingly obvious with increasing CDCR and SGS. The possible evolution of internal cracks for the grouted specimens was classified into three stages: (1) cracks initiating along the interfaces between the coal blocks and solidified grouts; (2) cracks initiating and propagating in coal blocks; and (3) cracks continually propagating successively in the interfaces, the coal blocks, and the solidified grouts near the coal blocks. Finally, after the propagation and coalescence of internal cracks through the entire specimens, there were two main failure modes for the failed grouted specimens. These modes included the inclined shear failure occurring in the more crushed coal rock and the splitting failure occurring in the less crushed coal rock. Both modes were different from the single failure mode along the fissure for the fractured coal rock after grouting solidification. However, compared to the brittle failure of intact coal rock, grouting into the different crushed degree coal rocks resulted in ductile deformation after the peak strength for the grouted specimens was attained.

Keywords: experimental investigation; mechanical behaviors; crushed coal rocks; grouting solidification

1. Introduction

Grouting is an extremely effective method for controlling groundwater inrush and reinforcing rock and soil masses that have low supporting capacity and high permeability in underground mining and engineering. To acquire a better understanding of the grouting mechanism for rock and soil materials, many experimental investigations have been carried out in recent decades (Voottipruex and Jamsawang 2014,Wang *et al.* 2016, Yang *et al.* 2014, Zheng *et al.* 2016). Among these studies, penetration grouting, merely requiring lower grouting pressure that is easy to control, has a wider application in practical underground engineering without disturbing the structure for the injected materials compared to compaction grouting or hydraulic fracturing. Dayakar *et al.* (2012) performed a permeation grouting laboratory experiment on the effect of cement grout in improving the supporting capacity of sandy soil, which showed that the increase of cement content improved the strength of the injected material. Mohtar *et al.* (2015) conducted experiments to study the penetration mechanism of bentonite grout injected into granular soils. The results indicated that the length of penetration of grouts decreased with a decrease in the W/B ratio and with an increase in the apparent viscosity of the grout.

In these experimental studies, most of the injected media are soils, whereas there are inadequate studies on grout permeation in fractured rocks because of the complexity of their fracture geometries and distribution (Xue 2015). The sealing effect of permeation grouting into a specimen fracture and the patterns of grout propagation were experimentally studied under water flow conditions (Sui *et al.* 2015). These authors analyzed the influence of different factors on the compaction effect, including the initial water flow speed, the aperture width of the fracture, the grout take and the gel time, among which the factor with

*Corresponding author, Professor
E-mail: hanlj@cumt.edu.cn

ISSN: 2005-307X (Print), 2092-6219 (Online)

the greatest influence was the aperture width. In addition, the grouting pressure increased gradually with the increase of grouting time during the grouting with water flowing. However, this experiment, based on similar material made with a transparent fracture replica, was obviously different from that of real rock from nature, which is complex and variable. Funehag and Fransson (2006) performed extensive experimental studies and in situ measurements on the penetration grouting into fractured natural rocks with silica sol and obtained the diffusion radius of grouts, considering the grouting pressure, the aperture width of the fracture and the material properties. Mohammed *et al.* (2015) investigated the cement-grout penetration through rock fractures under static and oscillatory conditions. These authors revealed that the grout flow with dynamic injection was faster than that with static pressure.

However, to date, compared to these studies on rocks containing fissures, few laboratory experiments have been performed on grouting into crushed rocks. As is well known, coal rock is a special kind of brittle rock, and crushed coal rocks after mining operations are widely distributed during underground mining, particularly in the coal crushing zone in a mine. However, these crushed coal rocks urgently need to be reinforced to improve their strength due to their extremely low supporting capacity. Grouting is a main method to reinforce these rock, whereas experimental results regarding permeation grouting into crushed coal rock are rare; the reasons for this lack are the difficulty of sampling crushed coal rocks from actual engineering projects and the inconvenience, due to the broken characteristics of crushed coal rocks, of recreating and testing such specimens using laboratory equipment (Zhou *et al.* 2015).

Moreover, the properties of grouts also have important influence on grout permeation in injected materials. Saric *et al.* (2003) investigated the performance characteristics of cement grouts containing different combinations of high-range water reducing agent and cellulose-based viscosity modifier. These authors summarized the effects of viscosity on the rheological characteristics of grouts. In addition, the strength, pore-size distribution and microstructural properties of the grouts were determined in this study. Khayat *et al.* (2008) carried out experiments to evaluate the influence of different types of supplementary cementitious materials (SCMs) on rheological properties, stability, as well as compressive strength of the structural grout. Mohammed *et al.* (2014) studied the rheological characteristics of cement-based grouts containing talc or palygorskite. These authors found that the fluidity of grout was positively affected by talc and negatively by palygorskite and early cement hydration. Gopinathan and Anand (2017) investigated the properties of cement grouts including flowability, bleeding, compressive strength and shrinkage. The results showed that, cement replacement with slag in grouts could decrease bleeding substantially without affecting the workability of mixtures, and slag enhanced the compressive strength and reduced shrinkage reasonably. Rahman *et al.* (2015) studied the rheological properties of commonly used cement grouts by using the Ultrasound Velocity Profiling combined with the Pressure Difference (UVP + PD) method. The results showed that the method was convenient to determine the rheological properties, and the variations with concentration and time. In these experiments, which mainly concentrated on the variations in the rheological properties and the strength of grouts during grouting, no attention was paid to the effects of the solidified grout strength on the mechanical characteristics of the grouted soil and rocks.

Previous experiments on permeation grouting into rocks have provided no satisfactory answers about the grouting reinforcement effects for grouted rocks, especially crushed coal rocks. These experiments have mainly been confined to paying attention to the parameters associated with the grout permeation mechanism, such as the diffusion distance of grout, the grouting pressure and the grouting time, which could not better reveal the reinforcement effect based on the mechanical characteristics of the grouted specimen. Therefore, in this paper, we performed a series of grouting tests on grouting into crushed coal rocks and considered the mechanical properties for the grouted specimens by using a independently developed laboratory apparatus having the advantages of easy disassembly and convenient recreating of the specimen compared with previous grouting experimental equipment (Suits *et al.* 2011,Wang *et al.* 2013). Based on the experimental results, we first studied the influences of the crushed degree of coal rock (CDCR) and the solidified grout strength (SGS) after different curing periods on the strength and deformation parameters of the grouted specimen for crushed coal rocks. Then, we present a reasonable crack evolution process to explain the initiation and propagation of cracks in the grouted specimen. Finally, the failure characteristics of deformed grouted specimens of the crushed coal rocks are analyzed in detail and compared with those coal rocks merely having partial fractures. Moreover, unlike existing studies that rarely consider the ground stress field, a hydraulic servo testing machine was used in our study to approximately simulate the ground stress in a real engineering environment.

2. Materials and methods

2.1 Materials used in experiments

The microfine cement grouts (W/C ratio of 0.85) are selected in the experiment, which has been widely applied in the reinforcement of underground engineering in the past few decades due to its more stable physical and mechanical properties, greater range of strength adjustability and better permeability, as well as its non-polluting nature. Fig. 1 shows the grain size distribution curves of three kinds of cements including fly ash cement (P.F 32.5), ordinary Portland cement (P.O 52.5) and microfine cement (1250(D90)). The results demonstrate that the average grain size of fly ash cement is the largest and its grain mass percentage for grain sizes below 30 μm is only 18.2%, compared to 65.1% and 88.4% for the ordinary Portland cement and the microfine cement, respectively, which indicates that the grouts made of microfine cement can penetrate into smaller voids more easily than the other two kinds of cement grouts because the former contain substantial amounts of tiny cement grains.

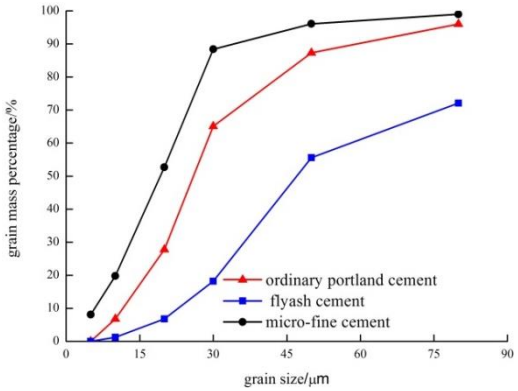

Fig. 1 Grain size distribution curves of three kinds of cements

Table 1 Selected mechanical parameters for the specimens of intact coal rocks and sandstone

Specimen	D (mm)	H (mm)	E (Gpa)	UCS (MPa)	R (MPa)
M-1	49.23	101.01	1.54	11.67	1.52
M-2	48.72	101.55	1.61	7.50	1.42
M-3	49.70	101.89	1.58	9.08	0.85
M-4	49.22	101.20	1.05	7.60	0.69
Sandstone			10-61		

*D: Diameter; H: Height; E: Elastic modulus; P: Poisson's ratio; UCS: Uniaxial compressive strength; R: Residual strength

The coal rock specimens from the Zhaozhuang mine, Shanxi province, China, were used in our study, which have anisotropic structures and an average density of approximately 1420 kg/m^3 and show the characteristics of greater brittleness, lower elastic modulus, easier crushability and greater compressibility compared with the ordinary rock (e.g., sandstone) given in Table 1. In addition, we experimentally measured the uniaxial compressive strength of intact coal rocks with a size of 50 mm in diameter and 100 mm in height, which were the same sizes as those of the grouted crushed coal rock, to contrast between the two kinds of coal rocks (intact and grouted crushed coal rocks) in some mechanical properties. To obtain the best possible results for the uniaxial compressive strength of the intact coal rock, we repeated the compression tests with several specimens having the same size (see Table 1).

2.2 Experimental setup

Fig. 2(a) shows a picture of the experimental setup, which consists mainly of a uniaxial compression system, a grouting test system, a grout supply system, a pipe system, and pressure gauges. The schematic layout of this experimental setup is as shown in Fig. 2(b). Moreover, the internal structure of the main grouting test system including the cylindrical grouting barrel, permeable stone, high-strength bolts and bottom plate is shown in Fig. 3.

A controllable grouting pump producing the grouting pressure was used to inject the microfine cement grouts

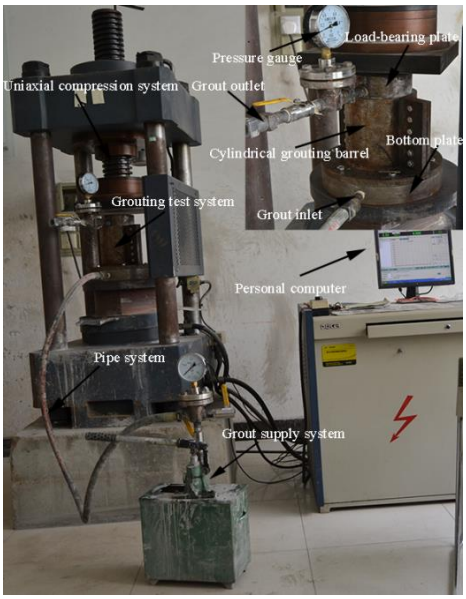

(a) Part of the penetration grouting experimental setup

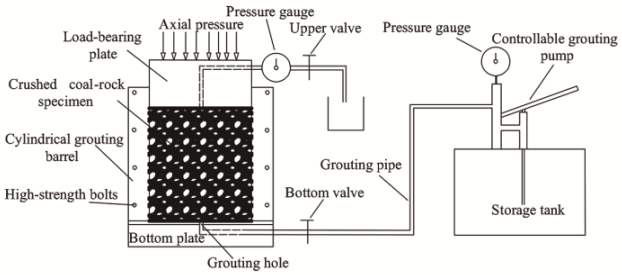

(b) Schematic layout of the laboratory test setup

Fig. 2 Grouting experimental setup

from the storage tank into the crushed coal rock specimen in the cylindrical grouting barrel (Fig. 2(b)). The pump had a pressure gauge to measure the grouting pressure, whose maximum value was 1 MPa in accordance with the experimental design requirement, and to provide a reference for controlling the grouting pressure. In addition, another pressure gauge near the grout outlet was applied to test the internal pressure in the grouting barrel.

The grouting test system was composed mainly of three components: a bottom plate, a cylindrical grouting barrel and a load-bearing plate (see Fig. 3). A grouting hole connected to a grouting pipe was centered in the bottom plate. In addition, the grouting pipe was attached to the hole in the bottom plate at one end and to the grouting pump at the other end and was used for transporting grouts from the grout storage tank to the experimental specimen placed in the grouting barrel, under the action of the grouting pressure. The cylindrical grouting barrel on the bottom plate with dimensions of 50 mm in inner diameter and 100 mm in height was assembled by two pieces of semi-cylindrical barrels using the high-strength bolts, which made for easy installation and disassembly when placing and removing the experimental specimen, respectively, as shown in Fig. 3(a). It should be noted that there was a permeable stone (see Fig. 3(b)) between the grouting barrel and the bottom plate to prevent small coal rock fragments from blocking the grouting hole.

A load-bearing plate of 50 mm in diameter could slide in

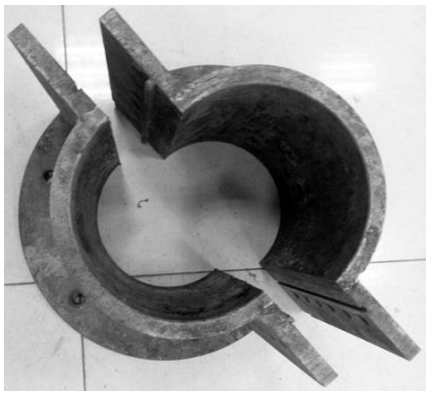

(a) Cylindrical grouting barrel assembled by two pieces of semi-cylindrical barrels

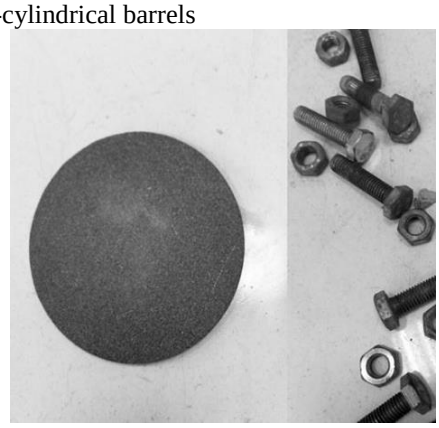

(b) Permeable stone and high-strength bolts

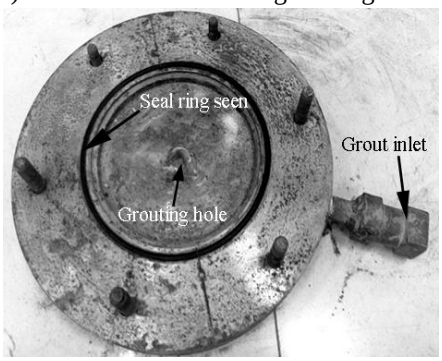

(c) Bottom plate

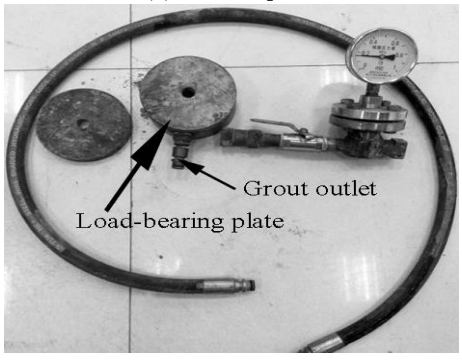

(d) Load-bearing plate, grouting pipe and pressure gauge

Fig. 3 Internal structures of the grouting test system

the grouting barrel at the top of the specimen and was used to transmit the axial pressure from the hydraulic servo testing machine to the test specimen with to imitate the ground stress in real underground mines.

Two valves were located at the inlet and outlet of grouts to adjust the grouts flowing into and out of the specimen, respectively. To be more specific, during the grouting, the bottom valve was opened to let the microfine cement grouts into the experimental specimen as the upper load of the specimen from the hydraulic servo testing machine reached the design value (analyzed in detail in the next section). Meanwhile, the upper valve remained open in the process of penetration grouting into the test specimen. With the grouts constantly permeating into the specimen under the grouting pressure, the open spaces of the crushed coal rock specimen were gradually filled with the grouts. When the grouts flowed out of the outlet on the load-bearing plate (Fig. 3(d)), the upper valve was shut down immediately. The grouting specimen remained in the grouting barrel for a long period of time under a constant grouting pressure, ensuring the uniformity and sufficiency of grout diffusion within the specimen. The grouting apparatuses should be cleaned shortly after the grouting experiments to prevent the occlusion of the grouting pipes, grouting holes, grouting pump, etc.

A seal ring, seen in Fig. 3(c), was used to maintain the seal characteristic for the grouting device during the grouting experiment.

This experimental setup made it possible to inject grouts into the crushed coal rocks with different CDCR and SGS under axial pressure and lateral confinement, and the grouts not only flowed from bottom to top along the axial flow within the specimen but also diffused in a radial direction, depending on the distribution of the fracture (or the space) among the coal blocks. Moreover, this setup also provided the possibility of investigating the mechanism of grouting into other soils and rocks having characteristics similar to those of the crushed coal rocks for further analysis and discussion.

2.3 Design of experiments

Since the CDCR in nature is difficult to accurately and exhaustively determine, to better describe these, many experiments have been designed (Ma *et al.* 2018, Ma, Rezania, *et al.* 2017, Ma, Zhou, *et al.* 2017, Zhou *et al.* 2018). For example, they designed variable grain diameters of (a) 2.5-5 mm, (b) 5-10 mm, (c) 10-15 mm, (d) 15-20 mm and (e) mixed sizes for crushed mudstone specimens as well as other specimens. Based on this experiment, using a square-hole sieve (Fig. 4(a)), the crushed coal was separated into four groups with different grain size ranges, namely 5-10 mm, 10-20 mm, 20-30 mm and 30-40 mm, which were mixed into four crushing grades based on the weight ratio of different grain size (denoted as A, B, C and D, respectively, in the test names; see Table 2). For example, “A” means the highest crushed degree of the coal rock; “B, C and D” successively decrease in the crushed degree. The layered paving method of crushed coal rocks is adopted to ensure the uniformity and compactness of the spcimen before grouting. A specimen of crushed coal rock before grouting is shown in Fig. 4(b).

Uniaxial compressive strength tests for the solidified grouts formed at the curing time of 3, 5, 8, 14 and 28 days were carried out using the hydraulic servo testing machine.

(a) A square-hole sieve

(b) Experimental specimen of crushed coal rock before grouting

Fig. 4 Specimen preparation

Table 2 Four grades of crushed degrees of coal rock based on the weight ratio of different grain size

Block diameter/mm	A	B	C	D
5-10	100%	50%	33.30%	33.30%
10-20	/	50%	33.30%	33.30%
20-30	/	/	33.30%	/
30-40	/	/	/	33.30%

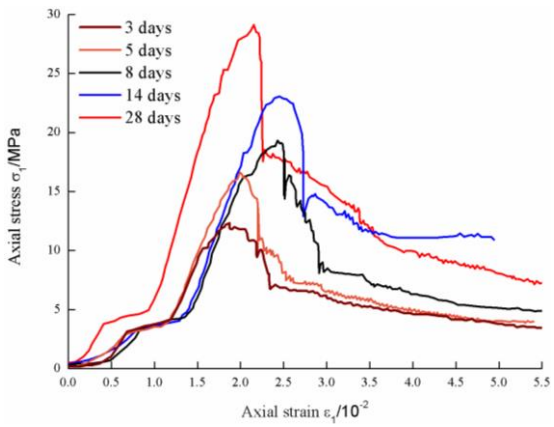

Fig. 5 Axial stress-strain curves of the solidified grouts after different curing times

Table 3 Mechanical strengths of solidified grout

T (d)	3	5	8	14	28
R_c (MPa)	12.3	16.6	19.3	23.0	29.1
Rt (MPa)	1.5	1.8	2.3	2.5	3.3

*T: Different curing times (days); R_c:Compressive strength; Rt:Tensile strengths

Fig. 6 Casting molds for making the specimens of the solidified grouts

These tests yielded 5 groups of strength values for solidified grouts (12.3, 16.6, 19.3, 23 and 29.1 MPa) corresponding to different curing times, as shown in Fig. 5. The values of σ_1 and ε_1 are the uniaxial compressive strength and the axial strain of the solidified grouts, respectively. Moreover, the tensile strengths of the grout are given in Table 3.

The casting mold used to make these specimens of solidified grouts, which had several advantages including convenient disassembly and good formability, was divided evenly into three parts with dimensions of 40×40×120 mm, as shown in Fig. 6. It should be noted that to investigate the influence of various SGS values on the mechanical characteristics of the grouted coal rock, the curing conditions of the specimen for solidified grouts from the casting molds (Fig. 6) and the specimen for grouted coal rocks were identical (both had the same curing times of 3, 5, 8, 14 and 28 days, as well as the same curing environment) to ensure that the strength of the solidified grouts from the casting molds could be used to express that of the solidified grouts within the grouted crushed coal rock.

To simulate the actual deep stress field situation as much as possible, lateral restraint is provided by the wall of the grouting barrel, and the ground stress is mainly represented by vertical stress, which can be approximately calculated as follows

$$\frac{F}{A} = \gamma H \tag{1}$$

where F and A are the axial pressure produced by the hydraulic servo testing machine and the area of load-bearing plate of 50 mm in diameter, respectively, and is the unit volume weight (approximately 14.2 KN/m^3 for this coal rock). In addition, H is the imitated formation depth.

Note that we approximately simulate the stress field at a depth of 211 m, relying on the actual engineering value, and a corresponding axial stress of approximately 2.8 MPa is required in this study.

3. Strength and deformation behaviors of the grouted crushed coal rocks

3.1 Axial stress-strain behaviors of the grouted specimens

Fig. 7 shows the axial stress-strain curves for the grouted specimens after different curing times of 3, 5, 8, 14 and 28 days (corresponding to SGS values of 12.3, 16.6, 19.3, 23 and 29.1 MPa) with four grades of CDCR ("Specimens A-D" represent the CDCR of the A-D grades, respectively; "1#- 5#" represent the SGS values of 12.3-29.1 MPa, respectively. For example, "Specimen A-1#" indicates the specimen with a CDCR of A grade and an SGS value of 12.3 MPa). It can be seen that the strength and deformation behavior of the grouted specimen depend greatly on the CDCR and SGS. In Fig. 7, σ_1 and ε_1 represent the axial stress and axial strain of the grouted specimen, respectively. It is worth noting that before the mechanical test, the top and bottom surfaces of the grouted specimen were ground smooth and then the rigid smooth spacers were placed on both surfaces to further reduce the end friction (Vaseline was also smeared between them to reduce friction).

From Fig. 7, it is clear that the axial stress-strain curves for different CDCR in the initial deformation stage have a favorable consistency at the SGS values of 12.3 and 16.6 MPa but a poor consistency at SGS values of 19.3, 23 and 29.1 MPa. This result indicates that in the initial stage, the CDCR has little effect on the mechanical behaviors of grouted specimens at the relatively lower SGS but has significant influence at higher SGS.

According to Fig. 7(a) and 7(b), we can determine that the grouted specimens have an initial nonlinear deformation, which results primarily from the compaction of pores containing residual air that is not forced out by the grouts but retained in the grouted specimen. After this stage, elastic deformation starts to dominate the axial stress-strain curves, and the axial stress remains in a similar linear relation with the axial strain. With the continuous increase of axial deformation, the stress-strain curves of the grouted specimens initially depart from linear behavior, which represents the yielding of the specimens. However, during the stage of yield deformation for the grouted specimen, minor stress drops occur, mainly due to the initiation of new cracks in the course of uniaxial loading. After the stress decreases, the grouted specimens quickly reach their peak strength. Meanwhile, the separation of curves begins to occur near the peak strength point, and the peak strengths gradually decrease with the decrease of the CDCR (except for Specimen D-1# in Fig. 7(a), which is explained in the next section), which indicates the CDCR has some impact on the peak strength of the grouted specimens in the initial damage stage. Note that after the peak strength, there are no obvious brittle failures, and the curves decline moderately, demonstrating that the crushed coal rock after grouting solidification has a good ductility that is conducive to maintaining structural stability when damage occurs. However, the axial stress-strain curve of the intact coal rock shows distinct brittleness (see Fig. 7(f)) after the peak strength, which is related to the mechanical characteristics of intact coal rock. Finally, the curves of grouted specimens approach each other gradually with approximately the same residual strength.

The higher the SGS becomes (Figs. 7(c)-7(e)), the more obvious the influence of the CDCR on the strength and deformation behaviors of the grouted specimen. In these figures, we can see that although the axial stress-strain curves (Figs. 7(c)-7(e)) have variations similar to those in Fig. 7(a) and 7(b) during the axial deformation including the voids compaction stage, elastic deformation and yielding deformation, the separation for curves is initiated at the beginning of axial deformation instead of near the peak strength point like Fig. 7(a) and 7(b). This result indicates that the consistency of the mechanical properties in these grouted specimens has been weakened with the SGS values from 12.3 to 29.1 MPa. The peak strengths decrease dramatically with the decrease in the CDCR, which results from the increase in the SGS. In addition, contrasting with the relatively concentrated peak point at a strain of approximately 0.012 in Fig. 7(a) and 7(b), the curves in Figs. 7(c)-7(e) show more dispersed peak points corresponding to a range of strains from 0.005 to 0.015. However, the grouted specimens at higher SGS also fail more slightly than the intact coal rock after the peak strength as the axial deformation increases. Therefore, the grouted specimens with the relatively greater SGS values (19.3, 23, and 29.1 MPa) still have excellent ductility similar to that of grouted specimens having lower SGS (12.3 and 16.6 MPa).

It should be noted that the peak strength of each grouted specimen with different CDCR and SGS ranging from 12.3 to 29.1 MPa is higher than the residual strength of the intact coal rock (see Fig. 7(f) and Table 1). This observation demonstrates that the permeation grouting can obviously reinforce the strength of the crushed coal rock under the conditions of ground stress in practice.

3.2 Effect of CDCR and SGS on the strength and deformation parameters of the grouted specimens

Table 4 lists the corresponding partial mechanical parameters of the grouted specimens after axial compression. In Table 4, σ_c and ε_c are respectively defined as the uniaxial compressive strength (UCS) and the peak axial strain of the grouted specimen, and E_S represents the static elastic modulus of the grouted specimen. Note that E_S is defined as the average slope of the line in the approximately linear elastic deformation stage of the stress-strain curves (Fig. 7). Based on the experimental data for the grouted specimens after axial compression listed in Table 4, Fig. 8 distinctly displays the relationship between the UCS in the grouted specimen and the different CDCR and SGS. According to Fig. 8, for the same CDCR, the UCS of the grouted specimens generally increases with the increase in the SGS. However, the four curves all first increase relatively rapidly and then slightly at SGS values from 19.3 to 23.0 MPa. This result indicates that the growth

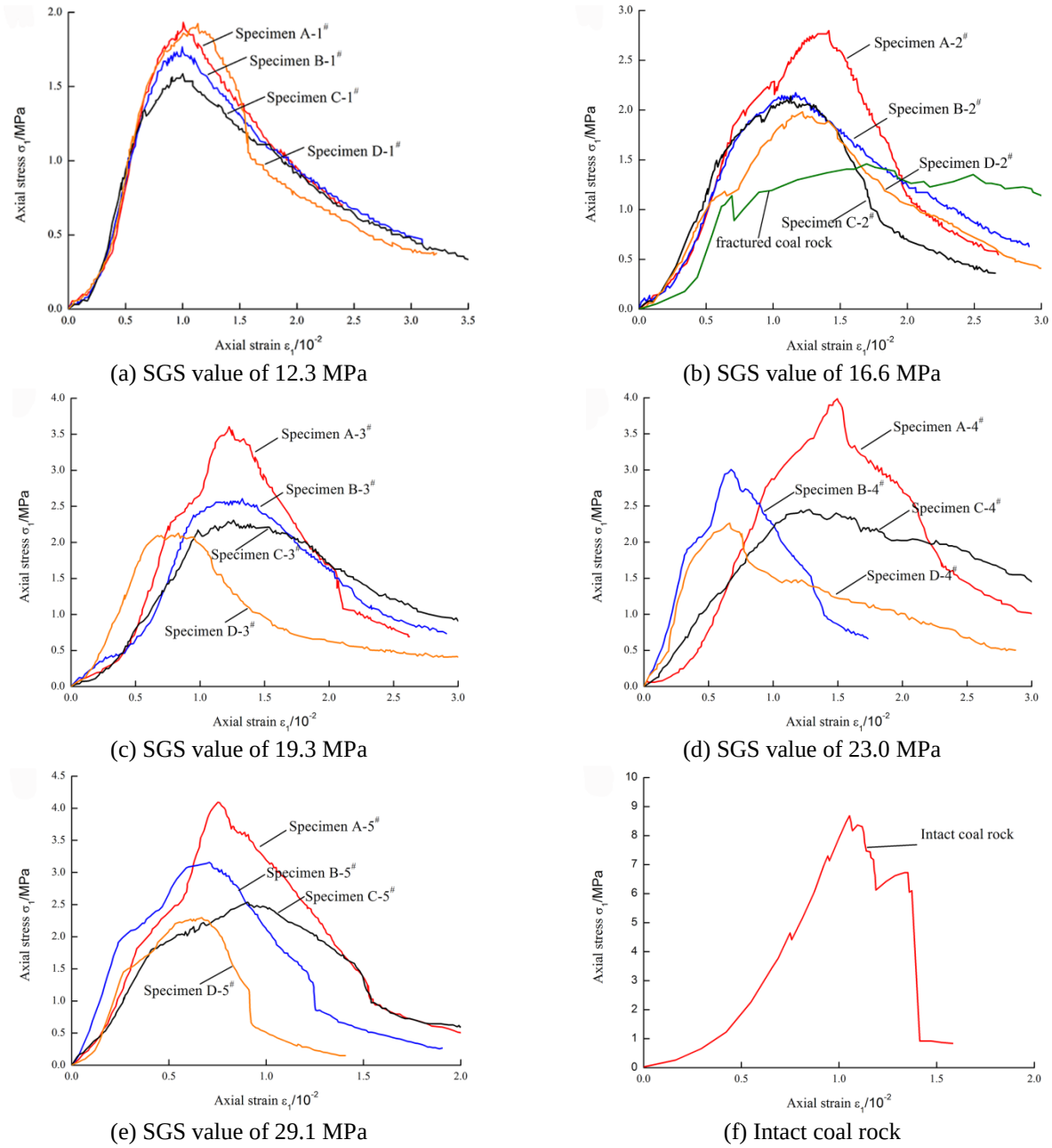

Fig. 7 Axial stress-strain curves for grouted specimens with different CDCR and SGS, and intact coal rock

rates of these curves for different CDCR at lower SGS (less than 19.3 or 23.0 MPa) are larger than those at higher SGS, especially for the more crushed coal rocks such as the coal rocks with A- and B-grade degrees of crushing. Therefore, we determine that the most reasonable range of SGS for the reinforcement effect in the grouted specimen is between 19.3 and 23.0 MPa. The SGS in this range not only ensures the strength of the grouted specimen but also saves experimental time (corresponding curing times between 8 and 14 days are far less than the longest design curing time of 28 days for SGS of 29.1 MPa), which is beneficial for the current laboratory testing, as well as for the related practical engineering.

Moreover, for the same SGS, the higher the CDCR is, the greater the UCS. However, for the grouted specimen with an SGS of 12.3 MPa listed in Table 4, as the CDCR decreased from A to B, the UCS of the grouted specimen decreased from 1.93 to 1.77 MPa and to 1.58 MPa at C. In contrast, when the CDCR decreased from C to D, the UCS increased suddenly from 1.58 to 1.92 MPa. That is, the UCS first decreased and then increased with the decrease in the crushed degree of specimen, rather than linearly decreasing consistently. This behavior was different from those for the other four SGS values of 16.6, 19.3, 23.0 and 29.1 MPa (see Table. 3 and Fig. 8), and the reasons are explained as follows.

For the SGS of 12.3 MPa, the superfine-cement grouts coagulated in the grouted specimens with the greater CDCR. These grouts easily formed a skeleton structure that can produce the skeleton supporting effect, which

Table 4 Strength and deformation parameters of the grouted specimens

Specimen	CDCR	SGS/MPa	*Es* /GPa	σ_c/MPa	ε_c
A-1#	A	12.3	0.376	1.93	1.005
A-2#	A	16.6	0.426	2.80	1.415
A-3#	A	19.3	0.531	3.60	1.226
A-4#	A	23.0	0.438	3.99	1.496
A-5#	A	29.1	0.702	4.09	0.752
B-1#	B	12.3	0.295	1.77	0.996
B-2#	B	16.6	0.340	2.17	1.167
B-3#	B	19.3	0.466	2.61	1.328
B-4#	B	23.0	0.727	3.01	0.675
B-5#	B	29.1	0.905	3.16	0.707
C-1#	C	12.3	0.304	1.58	1.001
C-2#	C	16.6	0.305	2.14	1.132
C-3#	C	19.3	0.268	2.31	1.260
C-4#	C	23.0	0.227	2.45	1.280
C-5#	C	29.1	0.547	2.54	0.904
D-1#	D	12.3	0.359	1.92	1.132
D-2#	D	16.6	0.264	1.98	1.219
D-3#	D	19.3	0.421	2.13	0.832
D-4#	D	23.0	0.676	2.26	0.663
D-5#	D	29.1	0.891	2.30	0.669

*Specimen represents grouted specimen; CDCR: Crushed degree of coal rock; SGS: Solidified grout strength; D: Diameter; H: Height; *Es*: Static elastic modulus; σ_c: Uniaxial compressive strength (UCS); ε_c: Peak axial strain

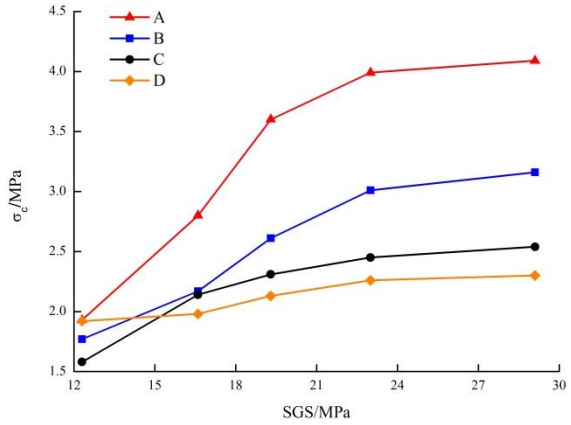

Fig. 8 Relationship between the UCS in the grouted specimen and different CDCR and SGS

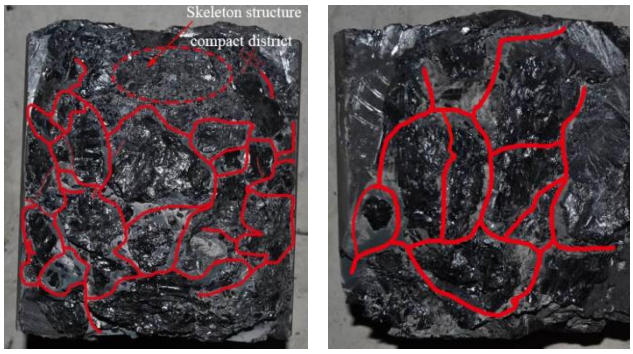

(a) (b)

Fig. 9 Cutting planes of the skeleton structure produced by the solidified grouts. (a) Skeleton structure in a grouted specimen with higher CDCR; (b) Skeleton structure in a grouted specimen with lower CDCR

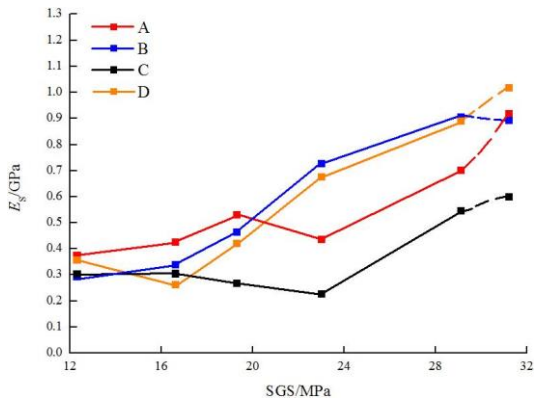

(a) Static elastic modulus

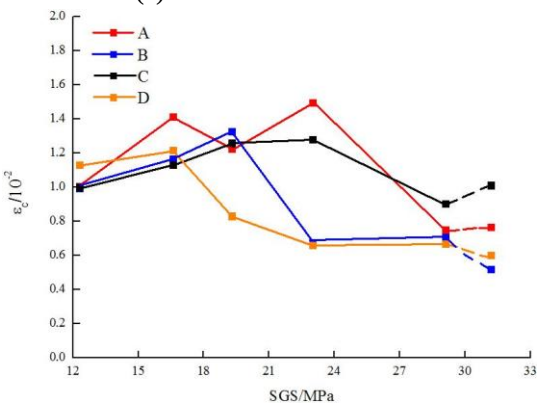

(b) Peak axial strain

Fig. 10 Influence of the CDCR and SGS on the elastic modulus and the peak axial strain of grouted specimens

dominates the supporting ability of the grouted specimen. However, as the CDCR decreased, the effect of skeleton supporting from solidified grouts was weakened, as shown in Fig. 9, resulting in a reduction in the strength of the grouted specimen. Meanwhile, when the CDCR continuously decreased, the quantity of relatively large coal rock blocks increased gradually, which formed a new supporting body having a certain supporting ability among these coal blocks. When the supporting ability among coal blocks rather than the skeleton supporting effect of solidified grouts initially played a dominant role, a sudden increase in the strength of the grouted specimen resulted as the CDCR decreased from C to D. However, for other specimens (with SGS from 16.6 to 29.1 MPa), with the decrease in the CDCR, the skeleton supporting effect was also weakened but remained to play a major role in the supporting ability for the grouted specimen due to the increase in SGS. As a result, the UCS decreased sequentially depending mainly on the decrease in the skeleton supporting effect instead of on the supporting ability among coal blocks.

Fig. 10 shows the influence of the CDCR and SGS on the elastic modulus and the peak axial strain of grouted specimens. From Fig. 10(a), it can be seen at an SGS of 12.3 MPa, the *E*s of a specimen with an A-grade degree of crushing was 0.38 GPa and increased with the increase of SGS in the range of 12.3 to 19.3 MPa. In contrast, the *E*s decreased to 0.44 GPa at an SGS of 23.0 MPa and then increased rapidly to 0.70 GPa as the SGS continually increased from 23.0 to 29.1 MPa. Like the *E*s of the grouted specimen with an A-grade degree of crushing, the *E*s values of grouted specimens with C and D-grade degrees of crushing did not increase progressively with the SGS. Both values first decreased and then increased with the increase in SGS. The *E*s of specimens with a C-grade degree of crushing remained approximately unchanged with a value of 0.31 GPa as the SGS increased from 12.3 to 16.6 MPa but decreased to 0.23 GPa at an SGS of 23.0 MPa and then increased to 0.55 GPa for SGS values ranging from 23.0 to 29.1 MPa. Moreover, with the increase of the SGS from 12.3 to 16.6 MPa, the *E*s of specimens with a D-grade degree of crushing decreased from 0.36 to 0.26 GPa, having a minimum value at an SGS of 16.6 MPa. The *E*s value then increased from 0.26 to 0.89 GPa as the SGS increased from 16.6 to 29.1 MPa. However, the *E*s of grouted specimens having a B-grade degree of crushing increased consistently from 0.30 to 0.91 GPa as the SGS increased from 12.3 to 29.1 MPa (the specimen was the stiffest at an SGS of 29.1 MPa compared to the other three specimens). Although there were several decreases for some curves of the *E*s (e.g., A-, C- and D-grade degrees of crushing), all of the curves showed upward trends with the increase in the SGS. Moreover, there were relatively small values for the *E*s of specimens with different crushed degrees at lower SGS, but these became increasingly larger as the SGS increased, which implied that the skeleton supporting effect related to the *E*s was more obvious at higher SGS. With regard to the influence of the CDCR on the *E*s of grouted specimens, when the SGS was low (below 16.6 MPa), the *E*s of most specimens decreased with the decrease in the CDCR. This result indicated that the CDCR had a relatively obvious effect on the *E*s of specimens at lower SGS but little influence on those at higher SGS (especially above an SGS of 19.3 MPa; see Fig. 10(a)). According to Fig. 10(b), we can see that the curves for peak axial strain with different CDCR exhibited a slightly nonlinear decreasing trend from values between 0.996 and 1.132 (at SGS of 12.3 MPa) to those between 0.669 and 0.904 (at SGS of 29.1 MPa), indicating that the brittleness of the grouted specimens increased modestly when the SGS was increased.

Moreover, we add some mechanical tests for the grouted specimens with an SGS value of approximately 31.2MPa (more than one year of curing time), and the results show that the variation tendency of the elastic modulus and the peak axial strain has not changed significantly (see the dotted lines in Fig.10).

3.3 Crack evolution mechanism of the grouted specimens under uniaxial compression

In this section, we present the possible evolution process of internal cracks in the grouted crushed coal rock before failure under uniaxial compression (see Fig. 11) based on the axial stress-strain curves of grouted specimens shown in Fig. 7. The sequential damage modes of crack propagation for the grouted specimen before ultimate failure are analyzed in detail during the uniaxial compression, including (1) initial damage of the specimen with cracks initiating and propagating along the contact interfaces between the coal blocks and solidified grouts (Fig. 11(b)); (2) moderate damage of the specimen with cracks initiating and propagating within partial coal blocks (Fig. 11(c)); and (3) relatively serious damage of the specimen with cracks further propagating sequentially in the contact interfaces, the coal blocks, and the solidified grouts near the coal blocks (Fig. 11(d)). After the third stage, the ultimate failure of the grouted specimen occurs as the crack propagates and coalesces through the entire grouted specimen.

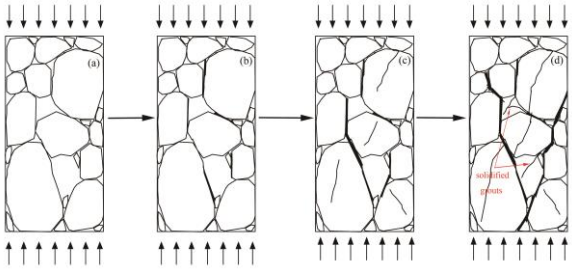

Fig. 11 Evolution process of the internal crack for a grouted specimen before the ultimate failure

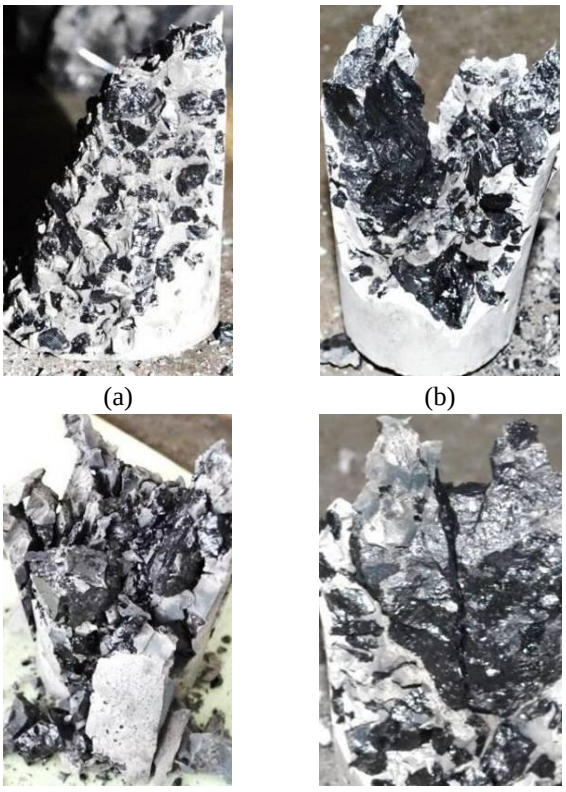

Fig. 12 Internal cracks and the damage to the grouted specimens under uniaxial compression. (a) and (b) Along the contact interfaces; (c) and (d) In partial coal blocks

The mechanism of crack propagation can be explained

as follows. In the initial damage of the grouted specimen as indicated in Fig. 11(b), there are several cracks at the contact interfaces between coal blocks and solidified grouts due to the low cohesive force of these contact interfaces because the resistance strength of the contact interfaces is smaller than that of the coal blocks and solidified grouts under uniaxial compression. For the second and third stages of crack propagation modes (Fig. 11(c) and 11(d)), after the cracks propagate in the contact interfaces between coal blocks and solidified grouts, the external load is shared together by coal blocks and solidified grouts with almost no cracks occurring at this time in the grouted specimen. However, for a certain region of the specimen, as the axial load increases and when the external load exceeds the strength of the coal blocks but is less than that of the solidified grouts near the coal blocks (Fig. 11(c)), new cracks begin to initiate primarily in the coal blocks. With the continual increase in the axial load, the propagation and coalescence of these cracks leads to the failure of the coal blocks. This failure then causes the solidified grouts near the coal blocks to start becoming the major structure supporting the load. When the stress concentration exceeds the strength of these solidified grouts, the cracks occur in the solidified grouts near the coal blocks (Fig. 11(d)).

Furthermore, Fig. 12 shows the internal damage modes of the grouted specimens. From Fig. 12(a) and 12(b), we can see that the main observed cracks and damage occur along the contact interfaces between the coal blocks and the solidified grouts. However, cracks propagate and coalesce in partial coal blocks in Fig. 12(c) and 12(d), which to some extent also verify the mechanism of evolution of crack in grouted crushed coal rock noted above (Fig. 11(c) and 11(d)). Note that the cracks and damage routes are approximately along the direction of axial stress.

3.4 Ultimate failure modes for the grouted specimens after uniaxial compression

The propagation of cracks extends to the nearby area and then results in macrocracks forming, which finally causes the total failure of the entire grouted specimen. There were two main failure modes in most of these grouted specimens in our laboratory experiments, including inclined shear failure and splitting failure. For example, Fig. 13 presents the failure modes of grouted crushed coal rocks and fractured coal rocks with the same SGS of 16.6 MPa for contrast under uniaxial compression. The inclined-shear failure modes mainly occurred in more crushed coal rock that had many interfaces between the coal blocks and solidified grouts, which was likely because the failure modes of the specimens were influenced simultaneously by the axial pressure and the skeleton structure of the solidified grouts. More specifically, the more crushed the coal rocks were, the more interfaces occurred between the coal blocks and the solidified grouts in the grouted crushed coal rocks. Then, with the increase in the axial load, the propagation and coalescence of a considerable number of cracks concentrating in the interfaces (note: cracks are apt to occur near interfaces) gradually formed a shear rupture zone. This process caused the inclined shear failure with relatively larger crack widths in the specimens under axial stress (see

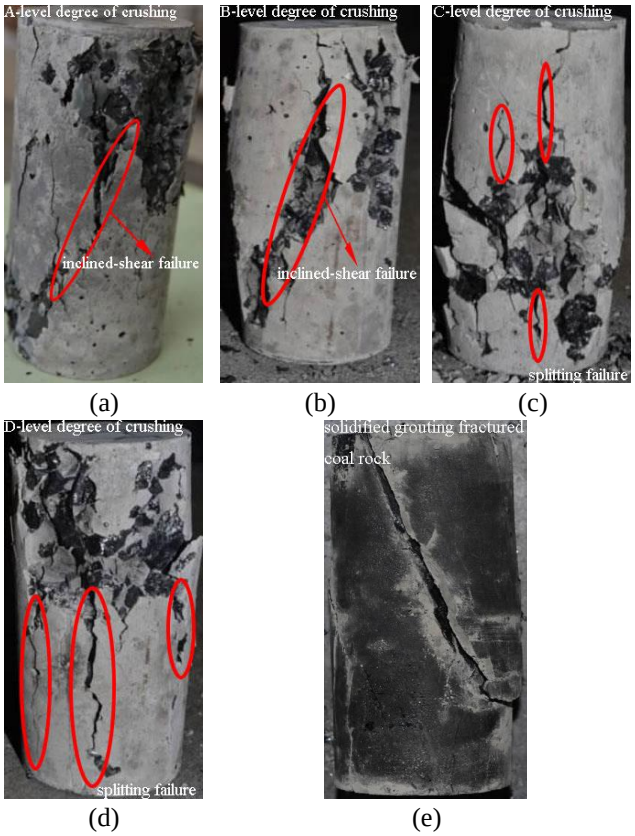

Fig. 13 Ultimate failure modes of the grouted crushed coal rocks and the fractured coal rock at an SGS of 16.6 MPa under uniaxial compression

Fig. 13(a) and (b)). When the CDCR was decreased, the size of coal blocks became larger, and the number of interfaces decreased. This combination led to the failure for the grouted specimens being primarily affected by the axial stress rather than both the skeleton structure and the axial stress, and then, splitting failure occurred (see Fig. 13(c) and (d)). The stress states between the two failure modes were obviously different.

However, as for the fractured coal-rock specimens after grouting, the failure modes became relatively simple, and the failure path was only along the original fracture development direction because the skeleton structure of solidified grouts did not form (see Fig. 13(e)). As a result, there was a gentler change tendency in the deformation failure stage for the axial stress-strain curve (e.g., Fig. 7(b)). Furthermore, from Fig. 7(b) (SGS of 16.6 MPa), compared to the peak stress for the grouted specimens of crushed coal rocks, that for fractured coal specimens (1.46 MPa) was lower, but the ductility was better than those of grouted specimens for crushed coal rocks.

4. Limitations and discussion

4.1 Limitations and further study

Permeation grouting into coal rocks is difficult to simulate accurately in laboratory experiments, especially for crushed coal rocks, due to the difficulty of sampling

from the real engineering space. Moreover, the simulation of ground stress in practice during the grouting injection process has not been well considered. For solving these problems, independently developed grouting equipment used to simulate permeation grouting into crushed coal rocks was applied in this research. A series of experiments on the mechanical behaviors of grouted coal rocks were conducted under uniaxial compression. However, for the experiment itself, some representative values of the CDCR and SGS were selected, which could not simulate more situations with different crushed degrees for coal rock and solidified grout strengths for the grouted coal rocks. Thus, a larger range of the CDCR and SGS should be considered in further study. Moreover, considering the representative element volume (REV), larger specimens should be used in experiments and numerical simulations to reduce the effect of specimen size on the mechanical behaviors of the grouted specimen. Furthermore, the microscopic failure behaviors and the grout diffusion characteristics for the grouted specimens should be investigated by X-ray CT scanning in future research.

4.2 Implications for grouting practice

Even with these limitations for the experiments, the findings from this research have some engineering implications for underground mining, particularly for the coal crushing zone in a mine. The CDCR and SGS have obvious influences on the mechanical behavior and the reinforcement effect of the crushed coal rock mass after grouting solidification. The optimum solidification strength for grouts was found to be between 19.3 and 23.0 MPa (instead of reaching the maximum strength of 29.1 MPa). These values were sufficient for the reinforcement of crushed coal rock masses in mining engineering, meaning shorter solidification time for practical engineering on the premise of ensuring the safety of construction. Moreover, the more crushed the coal rocks are, the more obvious the skeleton supporting effect is, which is beneficial for improving the mechanical properties of the crushed coal rocks after grouting. However, compared to the penetration grouting into the more crushed coal rocks, medium crushed coal rocks after grouting yield only a relatively weaker skeleton supporting effect. Based on the analysis above, some effective measures such as appropriately increasing the grouting volume and grouting range should be taken to improve the skeleton supporting effect in medium crushed coal rock masses after grouting. Furthermore, in a grouted engineering area with more crushed coal rocks, it is possible for ultimate failure to occur by inclined shear, and therefore, a composite supporting method (e.g., the combination of bolt support and grouting support) should be applied in such cases to reinforce the surrounding rock and prevent the inclined shear failure in the grouted coal rock mass.

5. Conclusions

To investigate the mechanical behaviors of crushed coal rocks after grouting and to consider the influences of different CDCR and SGS, several grouting and mechanical experiments have been conducted under uniaxial compression. Based on the results of the experiments, the following conclusions can be summarized as follows. When the SGS remained unchanged, the UCS of the grouted specimens decreased as the CDCR decreased (except at an SGS of 12.3 MPa). However, the UCS of grouted specimens having a constant CDCR increased as the SGS increased. We obtained the optimum solidification strength of the microfine cement grouts (between 19.3 and 23.0 MPa). Moreover, all of the UCS values for these grouted specimens were larger than the average residual strength of the intact coal rock, which demonstrated that the reinforcement effect of the crushed coal rock after grouting is quite obvious. The *E*s of grouted specimens with different CDCR indicated an upward trend with the increase in the SGS, whereas the peak axial strain with different CDCR showed a slightly nonlinear decreasing trend. This result indicated that the brittleness of the grouted specimens increased modestly with increasing SGS. However, the skeleton structures produced by the solidified grouts were weakened with the decrease in the CDCR and strengthened with the increase in the SGS. This condition had an important influence on the crack evolution and the ultimate failure modes in the grouted specimens. The possible internal cracks evolution mechanism of the grouted specimens under axial compression was proposed, including three main processes: (1) cracks initiating and propagating along the contact interfaces; (2) cracks propagating in partial coal blocks; and (3) cracks further propagating sequentially in the contact interfaces, the coal blocks, and the solidified grouts near the coal blocks. Subsequently, the ultimate failure of the grouted specimen occurred after the crack propagated and coalesced through the entire specimen. The two main failure modes in the failed grouted specimens included inclined shear failure and splitting failure, which were clearly observed in the current experiments.

The findings of this experimental investigation indicate the clear dependence of the deformation, strength, crack evolution, and failure mechanism of the grouted crushed coal rocks on the CDCR and SGS. Understanding the variation in the mechanical behaviors of the grouted crushed coal rocks will contribute to ensuring safe production in mining engineering, especially for the coal crushing zone in a mine.

Acknowledgments

This work was supported by the joint Ph.D. program of “double first rate” construction disciplines of CUMT. The first author (Ph.D. student of China University of Mining and Technology and visiting Ph.D. student of University of Nottingham) would like to acknowledge the anonymous reviewers for their valuable comments, which have greatly improved this paper.

References

Dayakar, P., Raman, K.V. and Raju, K.V.B. (2012), “Study on

permeation grouting using cement grout in sandy soil", *IOSR J. Mech. Civ. Eng.*, **4**(4), 5-10.
El Mohtar, C.S. and Rugg, D.A. (2011), "New three-way split mold design and experimental procedure for testing soft, grouted soils", *Geotech. Test. J.*, **34**(6), 1-13.
Funehag, J. and Fransson, Å. (2006), "Sealing narrow fractures with a Newtonian fluid: Model prediction for grouting verified by field study", *Tunn. Undergr. Sp. Technol.*, **21**(5), 492-498.
Gopinathan, S. and Anand, K.B. (2017), "Properties of cement grout modified with ultra-fine slag", *Front. Struct. Civ. Eng.*, **12**(1), 1-9.
Khayat, K.H., Yahia, A. and Sayed, M. (2008), "Effect of supplementary cementitious materials on rheological properties, bleeding, and strength of structural grout", *ACI Mater. J.*, 1**05**(6), 585-593.
Ma, D., Cai, X., Zhou, Z.L. and Li, X.B. (2018), "Experimental investigation on hydraulic properties of granular sandstone and mudstone mixtures", *Geofluids*.
Ma, D., Rezania, M., Yu, H.S. and Bai, H.B. (2017), "Variations of hydraulic properties of granular sandstones during water inrush: Effect of small particle migration", *Eng. Geol.*, **217**, 61-70.
Ma, D., Zhou, Z.L., Wu, J.Y., Li, Q. and Bai, H.B. (2017), "Grain size distribution effect on the hydraulic properties of disintegrated coal mixtures", *Energies*, **10**(5), 612.
Mohammed, M.H., Pusch, R., Knutsson, S. and Gunnar, H. (2014), "Rheological properties of cement-based grouts determined by different techniques", *Engineering*, **6**(5), 217-229.
Mohammed, M. H., Pusch, R. and Knutsson, S. (2015), "Study of cement-grout penetration into fractures under static and oscillatory conditions", *Tunn. Undergr. Sp. Technol.*, **45**, 10-19.
Mohtar, C.E., Yoon, J. and Elkhattab, M. (2015), "Experimental study on penetration of bentonite grout through granular soils", *Can. Geotech. J.*, **52**(11), 1850-1860.
Rahman, M., Håkansson, U. and Wiklund, J. (2015), "In-line rheological measurements of cement grouts: Effects of water/cement ratio and hydration", *Tunn. Undergr. Sp. Technol.*, **45**, 34-42.
Saric, C.M., Khayat, K.H. and Tagnit, H.A. (2003), "Performance characteristics of cement grouts made with various combinations of high-range water reducer and cellulose-based viscosity modifier", *Cement Concrete Res.*, **33**(12), 1999-2008.
Sui, W.H., Liu, J.Y., Hu, W., Qi, J.F. and Zhan, K.Y. (2015), "Experimental investigation on sealing efficiency of chemical grouting in rock fracture with flowing water", *Tunn. Undergr. Sp. Technol.*, **50**(1), 239-249.
Voottipruex, P. and Jamsawang, P. (2014), "Characteristics of expansive soils improved with cement and fly ash in Northern Thailand", *Geomech. Eng.*, **6**(5), 437-453.
Wang, Q., Wang, S., Sloan, S.W., Sheng, D.C. and Pakzad, R. (2016), "Experimental investigation of pressure grouting in sand", *Soil. Found.*, **56**(2), 161-173.
Wang, S.Y., Chan, D.H., Lam, K.C. and Au, S.K.A. (2013), "A new laboratory apparatus for studying dynamic compaction grouting into granular soils", *Soil. Found.*, **53**(3), 462-468.
Xue, X.H. (2015), "Study on relations between porosity and damage in fractured rock mass", *Geomech. Eng.*, **9**(1), 15-24.
Yang, Z.Q., Hou, K.P., Wei, L., Yong, C. and Yang, B.J. (2014), "Study of diffusion parameters of Newtonian fluid based on column-hemispherical penetration grouting", *Rock Soil Mech.*, **35**(S2), 47-53.
Zheng, G., Zhang, X.S., Diao, Y. and Lei, H.Y. (2016), "Experimental study on the performance of compensation grouting in structured soil", *Geomech. Eng.*, **10**(3), 335-355.
Zhou, J. W., Liu, Y., Du, C.L. and Wang, F.R. (2015), "Experimental study on crushing characteristic of coal and gangue under impact load", *Int. J. Coal. Prepar. Utiliz.*, **36**(5), 272-282.
Zhou, Z.L., Cai, X., Ma, D., Cao, W.Z., Chen, L. and Zhou, J. (2018), "Effects of water content on fracture and mechanical behavior of sandstone with a low clay mineral content", *Eng. Fract. Mech.*, **193**, 47-65.

CC